Polyaxial Figures of the Moon

Research article

H. Bâki İz 1*, X.L. Ding 1, C.L. Dai2, C.K. Shum2

- 1 Dept. of Land Surveying and Geo-Informatics The Hong Kong Polytechnic University Hong Kong, China
- 2 Division of Geodetic Science School of Earth Sciences The Ohio State University USA

Abstract:

This study investigates various models to represent the gross geometric shape of the Moon. Asymmetric polyaxial geometric models-namely three-, four- and six-axial lunar figure - are compared and contrasted with the axially symmetric three-axis ellipsoidal model derived from Chang'e 1 and SELENE laser altimetry data. All solutions confirm a hydrostatically stable lunar shape shifted with respect to the lunar center of mass by topography. Model solutions with increasing complexity offer additional information about the regional properties of the lunar topography. Solution statistics suggest that axially symmetric lunar figures and their center of figure parameters can be replaced by an equivalent asymmetric lunar shape centered at the center of mass of the Moon. Thus, using only three shape parameters, one can derive an "egg" shape that better accommodates the true geometry of the Moon.

Kevwords

Polyaxial Lunar Figure • Lunar Laser Altimetry • Lunar Orientation • Change'E-1 • SELENE © Versita sp. z o.o.

Received 03-08-2011; accepted 09-09-2011

1. Introduction

Isolated self-gravitating massive objects are spherically symmetric, which minimizes potential energy. Their steady rotation distorts their spherical shape, a hydrostatic departure which is characterized by even degree zonal spherical harmonics (Bills and Lemoine, 1995). Meanwhile, the topography and internal structure of a planet displaces its center of figure from its center of mass. Earlier studies by Sjogren and Wollenhaupt (1973) revealed the displacement of the center of figure of the Moon relative to the center of mass using laser altimetry. This offset is subsequently quantified by the first-degree harmonic term of lunar topographic model solutions (Bills and Ferrari, 1977, Smith et al., 1997). The displacement is attributed to the asymmetry of topography, the uneven distribution of mare, the greater thickness of the highland anorthositic layer on the far side, or the composition and structure of the lunar interior (Kaula et al., 1972, Wieczorek et al., 2006).

If spherical shapes are the first-order approximations to the gross

shape of the Moon, symmetrical two-axial (rotational) or three-axial ellipsoids approximate its hydrostatically stable figure. Although lunartopography and shape can be completely described by a sufficiently high-degree and -order spherical harmonic topographic model (Ping et al., 2003, Araki et al., 2009) and the deviations from the symmetry can be deduced from low-degree and -order harmonic coefficients of such solutions, this study will show that asymmetric ellipsoids can serve as alternative models. The parameters of these figures offer additional constraints in investigating the internal composition and structure of the Moon. On the other hand, performing a best fit of geometric lunar figures with fewer parameters is preferable in lunar mapping for computational efficiency reasons.

In the following sections, alternative asymmetric geometric models for the lunar figure is formulated. Their parameters are estimated from the recent Chang'e-1 and SELENE laser altimetry data; these parameters are then compared with the parameters estimated for symmetrical three-axial ellipsoidal models.

^{*}E-mail: lshbiz@polyu.edu.hk



Journal of Geodetic Science

2. Axially Symmetric Lunar Figure

Recent approaches in determining lunar figure parameters use a spherical harmonic representation of the lunar topography. As early as 1977, Bills and Ferrari calculated the axes of a three-axial lunar ellipsoid using a spherical harmonic analysis of lunar topography to degree 12 from Earth-based and orbital observations. In a follow up study, Smith et al. (1997) derived a Goddard Lunar Topography Model (GLTM 2) up to degree and order 72 based on a spherical harmonic expansion of the mass-centered radii deduced using Clementine radar altimetry measurements. GLTM 2 models were then used to compute the parameters for a biaxial and spherical lunar shape.

Most recently, two-axial lunar figure parameters and their geometric centers with respect to the lunar center of mass were derived based on the lunar spherical harmonic topographic model by Ping et al. (2009) from Chang'e-1, (CLTM-s01) topographic model with 3 million data. Concurrently, Araki et al. (2009) constructed the STM 359-grid-02 topographic model interpolated and filtered from 1.1 million SELENE laser altimetry measurements to a quarter of a degree. There are currently no published three-axial solutions derived from the recent topographic models based on spherical harmonic analysis.

Lunar figure parameters can also be obtained directly using geometric models. Iz (2009) calculated the parameters of the geometrically best fitting two-axial and three-axial ellipsoids and spheres from the coordinates of 271,610 ULCN 2005 lunar control stations (Archinal et al., 2006). Subsequently, Iz et al. 2009 showed that the omission of the topography in the old Unified Lunar Control Networks' ULCN 1994 solution (Davies, 1987) shifted the geometric center of the lunar figure up to 5 km in the lunar equatorial plane and rotated the ULCN 1994 reference frame on the order of a few hundred meters with respect to ULCN 2005 (at the lunar equator).

Recently, Iz et al. (2011) estimated improved spherical two- and three-axial lunar figure parameters together with their geometric centers with respect to the center of mass of the Moon, this time using Chang'e-1 and SELENE laser altimetry data. Another study by Iz et al. (2010) confirmed that the lunar polar axis is tilted toward the earth, as deduced earlier by Smith et al. (1997) from the analysis of the Clementine laser altimetry data.

3. Mathematical Models for Asymmetric Lunar Figures

Ellipsoidal geometric models are helpful for studying the Moon's topography, interior, and gross shape, but these models do not exactly correspond to laser altimetry observations. A more accurate representation of the lunar figure is possible using asymmetric polyaxial models (more than three axes), which have been deployed in planetary cartography for astronomical mapping of irregularly shaped celestial bodies (Stooke and Keller, 1990, Nyrtsov, 2005) but which have not been used to represent the gross shape of the Moon.

The simplest asymmetric polyaxial figure of the Moon is a three-axial ellipsoidal figure whose geometric center coincides with its center of mass (Fig. 1). This model is a fusion of two ellipsoids, one for representing the near side (a two-axis ellipsoid), the other for representing the lunar shape on the far side (a three-axial ellipsoid). These two differ only on the principal axes along the mean Earth direction (X-axis). In this formulation, having common axes ensures that the transition from the nearside to the far side is smooth (does not contain jumps).

The mathematical model of a four-axis version of such a composite figure consists of; a, the equatorial axis along the X-axis of the mean Earth/polar axis reference system on the near side; a', the equatorial axis on the far side; b, the other equatorial axis for both the near and the far side in the Y-axis; and c, which is the common polar axis that coincides with the Z-axis of the mean Earth/polar axis reference system. It is represented as

Near-side:

$$\frac{x^2}{a^2} + \frac{y^2}{b^2} + \frac{z^2}{c^2} - 1 = 0 \tag{1}$$

Far-side:

$$\frac{x^2}{a'^2} + \frac{y^2}{b^2} + \frac{z^2}{c^2} - 1 = 0$$
 (2)

Note that this model does not constrain the length of the axes with respect to each other, but it assumes that the center of mass and center of figure axes coincide and that the principal axes are all aligned with the axes of the underlying mean Earth/polar axis reference system. These models are differentiated in this study as models "without center of figure parameters", and "without orientation parameters" with italics.

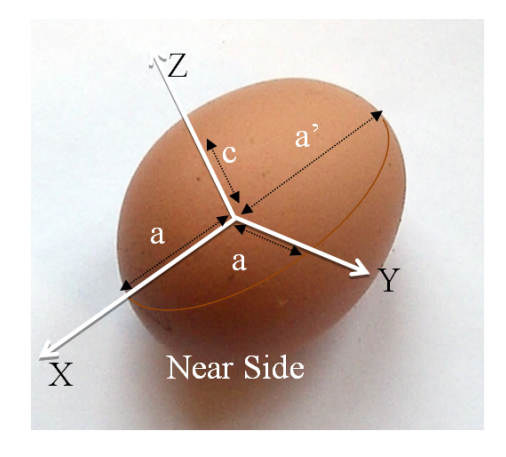


Figure 1. A four-axis (egg-shaped) representation of the lunar figure that differentiates the near from the far side of the Moon.

A variant of this model includes the position of geometric center of the four-axis ellipsoid with respect to the origin of the mean Earth/polar axis reference system, which coincides with the center of mass of the Moon;



Near-side:

$$\frac{(x-x_c)^2}{a^2} + \frac{(y-y_c)^2}{b^2} + \frac{(z-z_c)^2}{c^2} - 1 = 0$$
 (3)

Far-side:

$$\frac{(x-x_c)^2}{a'^2} + \frac{(y-y_c)^2}{b^2} + \frac{(z-z_c)^2}{c^2} - 1 = 0 \quad . \tag{4}$$

These models are described in this study as models "with center of figure parameters" and "without orientation parameters" with italics

The orientation of the above four-axial ellipsoidal figure of the Moon with respect to the mean Earth/polar axis reference system can also be modeled (to be estimated concurrently with the center of figure and shape parameters) using the formulations given by Iz et al. 2010:

Near-side:

$$(\mathbf{R}\Delta \mathbf{x})^{\mathsf{T}}\mathbf{N}(\mathbf{R}\Delta \mathbf{x}) - 1 = 0 \tag{5}$$

Far-side:

$$(\mathbf{R}\Delta \mathbf{x})^T \mathbf{F} (\mathbf{R}\Delta \mathbf{x}) - 1 = 0 \tag{6}$$

where

$$\mathbf{R} = \begin{pmatrix} 1 & 0 & 0 \\ 0 & \cos\alpha & \sin\alpha \\ 0 & -\sin\alpha & \cos\alpha \end{pmatrix} \cdot \begin{pmatrix} \cos\beta & 0 & -\sin\beta \\ 0 & 1 & 0 \\ \sin\beta & 0 & \cos\beta \end{pmatrix} \cdot \begin{pmatrix} \cos\gamma & \sin\gamma & 0 \\ -\sin\gamma & \cos\gamma & 0 \\ 0 & 0 & 1 \end{pmatrix}$$
(7)

$$\Delta \mathbf{x} := \begin{pmatrix} x - x_c \\ y - y_c \\ z - z_c \end{pmatrix}, \quad \mathbf{N} := \begin{pmatrix} a^{-2} & 0 & 0 \\ 0 & b^{-2} & 0 \\ 0 & 0 & c^{-2} \end{pmatrix}, \quad \mathbf{F} := \begin{pmatrix} a'^{-2} & 0 & 0 \\ 0 & b^{-2} & 0 \\ 0 & 0 & c^{-2} \end{pmatrix}$$
(8)

in which α , β , γ are the rotation angles of the lunar figure about the X ,Y, Z axes of the mean Earth/polar axis reference system, respectively, with an additional semi-major axis on the far side of the Moon. These models are described in this study as models "with center of figure parameters" and "with orientation parameters".

The above formulations can be extended to include additional lunar shape parameters. A six-axis geometric model, for instance, will consider the asymmetry with respect to the equatorial plane of the Moon by introducing two more axes, b' and c', along the Y and Z axes on the Western and Southern hemispheres. With the inclusion of these two new axes, the model will partition the lunar figure into eight quadrants. These quadrants can capture the effect of regional scale topographical features such as the South Pole-Aitken (SPA) region, and the highlands of the Eastern part on the far side (Figure 3), in estimating improved lunar shape parameters. They will also help to quantify the contribution of the residual lunar topography to the lunar shape parameters and to the orientation of the gross lunar figure.

In this study, various non-linear mathematical models, based on the variants of the condition equations (1) - (8) are used to iteratively estimate the relevant parameters of the lunar figure using the Cartesian coordinates of the laser altimetry footprints from Chang'e-1 and SELENE laser altimetry measurements. The least squares approach is used in solving condition equations with unknown parameters (see |z, (2009).

China Lunar Exploration Center provided the footprint locations of

over 8.5 million selenocentric laser altimetry measurements (after removing over 300,000 outliers). The radial distances of the laser altimetry footprints were calibrated by comparing them against the radial distances of the Lunar Laser Ranging (LLR) sites (Iz, et al. 2011). Japan Aerospace Exploration Agency (JAXA) (2009) provided over 8.8 million selenocentric SELENE laser altimetry measurements and their footprint locations. Statistical analysis of the laser altimetry footprint positions nearby the LLR station coordinates did not show any statistically significant differences (ibid). Because of this, no calibration correction was applied to the SELENE laser altimetry footprint radial distances.

To minimize the correlation among the parameters (lunar shape parameters and others),250,000 uniformly distributed laser altimetry measurements were sampled (regularized) using the random sampling approach on a unit sphere (ibid). They are used to estimate the unknown parameters for each data set rather than the whole data sets, which are increasingly dense toward the lunar poles due to the satellites' polar orbits.

Separate solutions are obtained to validate the solutions from Chang'e-1 and SELENE data against each other. The averaged values of the estimates are used for the analysis. Solutions with the fusion of the data sets do not differ from the averaged values, except scaling the variance factors, because of the well-known "square root n" effect.

Journal of Geodetic Science

4. Solution Comparisons

Table 1 lists estimates from various postulated geometric models of the Moon. These models either include center of figure parameters (with respect to the center of mass of the Moon) or ignore them in solving the gross shape parameters (models are denoted as with and without center of figure parameters). Common to all solutions is that the principal axes of the ellipsoids remain parallel to the underlying mean Earth/polar axis reference frame (i.e. the rigid body rotations of the ellipsoids are constrained to zero as opposed to solutions to models with rotation angles given in Table 2). Only the averaged values calculated from solutions using Chang'e-1 and SELENE laser altimetry data are listed in both tables. The root mean square (RMS) error values are the RMS residuals of the laser altimetry foot print Cartesian coordinates reflecting the quality of the fit for each model.

The standard errors of the estimates are less than 1 m for the principal axes and the geometric center parameters. Nonetheless, the standard errors do not reflect the accuracy of the estimated parameters since the expected value of the residual lunar topography is not zero. Although the Chang'e-1 and SELENE solutions are both calibrated against the coordinates of near side lunar ranging sites (|z et al., 2011), calibration only ensures the accuracy of the laser altimetry footprint coordinates on the near side of the Moon. The 53 m RMS value of the differences in the estimated parameters from Chang'e-1 and SELENE solutions displayed in Figure 2 can be used as a rough guideline for the accuracy of the estimate, which can be extended to approximately 160 m for a three-sigma error. Also note that all the geometric solutions in principle are biased for the same reason and the degree of bias depends on how well the lunar topography is incorporated into the geometric model, such as those estimated from the harmonic lunar topography models.

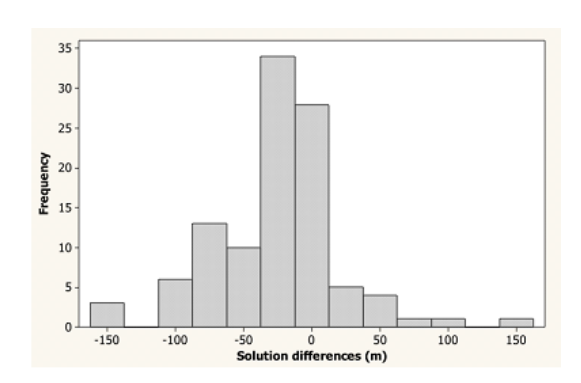


Figure 2. Histogram of the shape and center of figure parameters differences (Chang'E-1 - SELENE) estimated from eight different geometric models. The RMS of the differences is ± 53 m.

The estimated parameters reported by Smith et al. (1997) are also included in Table 1 and 2 to establish a baseline for the solutions with and without three-axial ellipsoid orientation parameters.

They were calculated from the spherical harmonic models of lunar topography using Clementine laser altimetry measurements. In both Clementine solutions, the origin of the three-axis ellipsoid is estimated independently by averaging the laser altimetry footprint in Cartesian coordinates. The Clementine mission solution with orientation is also reported to be a geometric solution as opposed to the solution without orientation parameters derived from the harmonic topography model.

Table 1 results show that there are large differences in the semi-principal axes of the ellipsoids from Clementine (Smith et al., 1997) and the other solutions mainly because of the missing laser altimetry measurements towards the poles. Nonetheless, the limited distribution of the data did not adversely affect the estimates of the center of figure parameters as evidenced by their agreement with the other center of figure estimates listed in the same table for the three-axis models using Chang'e-1 and SELENE data.

Note that the gross lunar shape, center of figure, and parameters are geometrically uncorrelated in the three-axis and symmetric models because of the globally distributed data as well as the geometric relationships between the shape and center of figure parameters. However, three-axis asymmetric and four- and six-axis shape parameters are all correlated with the corresponding coordinate components of the geometric center of the lunar figure. Semi-major axes on the near and far sides, for instance, are correlated with the X-coordinate component of the center of figure parameters. Consequently, the shape parameters estimated from solutions without center of figure parameters are biased in the corresponding axis by roughly the same length of the excluded component. For instance, the equatorial semi-major axis on the far side absorbs the unmodeled X-component of the center of figure parameters while the other shape parameters remain invariant.

In general the lengths of the polar axes (c and c') do not vary much from model to model. The inclusion of center of figure parameters always decreases the RMS error of the corresponding solution, yet the improvements are smaller for the six-axis solutions where additional shape parameters explain more variations in regional topography. The RMS error statistics of all solutions with center of figure parameters are very similar. In particular, the RMS error of three-axial asymmetric model (1887 m) with center of figure parameters is as good as the RMS error of the six-axial model with center of figure parameter solution (1884 m) if parsimony is a criterion in model selection. In this case, the three-axis model without the center of figure parameters is the parsimonious solution with only three shape parameters as compared to the others with only approximately 100 m increase in its RMS error as compared to the RMS error of other three-axis models.

Model solutions that also include lunar figure orientation parameters are listed in Table 2. The RMS error of these solutions decreases as the number of parameters in the models increases, as before, although the RMS error values do not vary for different models. In particular, solutions with center of figure parameters are pairwise

	Clementine	Three-axial (S)		Three-axial		Four-axial		Six-axial	
a	*1738056	1738056	1738046	1736974	1737652	1735871	1737825	1735872	1737825
a'				1740435	1738409	1740216	1738267	1740217	1738267
b	1737843	1737630	1737638			1737635	1737638	1736705	1737058
b'								1738568	1738217
С	1735485	1735691	1735689	1735690	1735688	1735690	1735688	1736015	1736428
c'								1735363	1734948
x _c	**-1740		-1727		-1443		-1561		-1561
у _с	-750		-716		-715		-715		-280
Z _c	270		224		224		224		-331
RMSE	-	2177	1886	1988	1887	1949	1887	1891	1884

Table 1. Three, four and six-axial lunar shapes with and without center of figure parameters (m) from the averaged estimates of the eight different geometric models using Chang'E-1 and SELENE laser altimetry data. The first three three-axial models are axially symmetric and denoted by (S).

better than those without them. Over all, the RMS error values for solutions with orientation angles are smaller than the ones without the orientation angles simply because of the implicit constraint built into the models listed in Table 2 by not allowing the lunar figure to rotate in searching for the best-fit solution. Table 2 also includes the estimates of the solutions with orientation angles. The latitudes and longitudes of the lunar South Pole (SP) position of the polar axis of the three-axis ellipsoid in the mean Earth / polar axis coordinate frame (calculated from the estimated rotation angles) are also listed in this table. The rotation angles for the Clementine solution were not reported by Smith at al. (1997). The standard errors of the estimated parameters are again less than 1 m for the lunar shape and for the center of the three-axis ellipsoid parameters, and less than 0.001 degrees for the rotation angles.

What is readily evident in the solutions with the orientation angles is the effect of the SPAimpact region, the largest known topographical feature in the solar system. As a result, the position of the South Polar axis in all solutions is located within the SPA region close to the center of its elliptical shape (Figure 3). Moreover, as the complexity of the model increases, the correlations among various parameters bias the center of figure estimates more and more. The interplay between parameters can be seen in the differences of the shape parameters. However, the results are still informative in assessing the lump sum distribution of topography and the gross changes in the lunar shape in different quadrants.

5. Conclusions

The results show that the lunar figure can be represented by different models; each one of these models is informative in its own way. In general, the figure axes do not deviate more than few km from each other for different models (Table 1 and 2), which confirms a hydrostatically stable lunar shape shifted with respect to the lunar center of mass by topography.

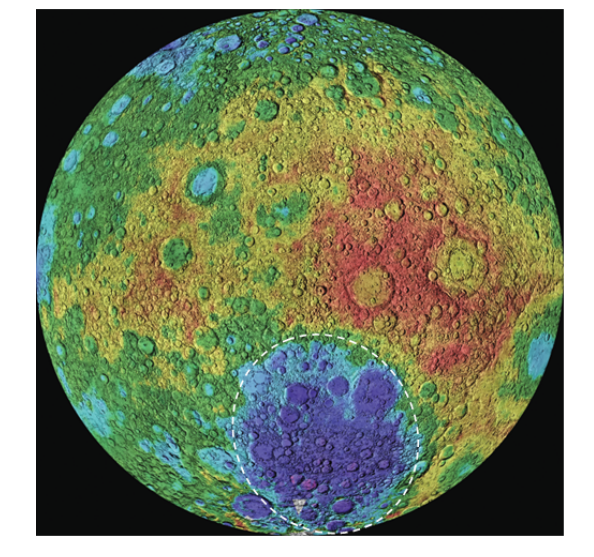


Figure 3. South Pole-Aitken Basin. Courtesy of the U.S. Geological Survey.

Constrained models (i.e. those without orientation parameters) are more consistent with each other, and the estimated center of figure of parameters are unbiased. Modeling the lunar figure by allowing it to rotate leads to solutions that are dominated by the South Pole-Aitken (SPA) region. These models are informative in investigating the Moon's evolution and interior as a function of its biggest impact region using different estimates of the polar flattening of each quadrant. Models with orientation parameters explain the lump sum variations of topography almost 30% better than the symmetric triaxial model.

All model parameters are ready to be analyzed in the context of the low degree and order coefficients of harmonic models of lunar



^{*} Clementine best fitting three-axial solution (Smith et al. 1997).

^{**}Center of figure parameters were calculated separately.

	Clementine	ne Three-axial (S)		Three-axial		Four-axial		Six-axial	
	Cicincina	entine Timee data (5)		Timee data		I TOUT UNION		JIX UXIUI	
a	*1739020	1738546	1739056	1737056	1737357	1736532	1737250	1737148	1737513
a'				1741637	1740749	1741532	1740815	1739911	1740593
b	1737567	1737500	1737354			1737369	1737378	1737336	1739221
b'								1737691	1735379
С	1734840	1735326	1734966	1734975	1734967	1734976	1734967	1735699	1739342
c'								1734964	1730717
X _c			-1727		-696		-643		-1406
Ус			-719		-189		-161		-1705
Z _C			223		-94		-109		-3285
α		17	17	19	20	19	20	19	9
β		21	21	17	18	17	18	16	22
γ		27	27	31	34	32	34	34	31
South Pole	66.005	62.745	62.675	64.505	63.225	64.625	63.28N	65.515	65.925
	169.60W	166.33E	166.44E	161.96E	165.02E	161.39E	164.86E	163.63E	172.63W
RMSE	-	2009	1690	1686	1662	1673	1662	1668	1565

Table 2. Three, four and six-axial lunar shapes with and without center of figure parameters (m) and with and without orientation parameters (degrees) from the averaged estimates of the eight different geometric models using Chang'E-1 and SELENE laser altimetry data.

topography.

And finally, as a result of this study, a parsimonious lunar geometric model arises with only three shape parameters; a two-axis nearside ellipsoidal representation (semi-major and polar axes a and c), and a three-axis ellipsoid (semi-major axis a', minor axis a, and the polar axis of the far side of the Moon c). These parameters represent a significant portion of the Moon's gross shape and its topography and its near and far side dichotomy.

Acknowledgement

This study is supported by Hong Kong Polytechnic University grants G-U417 and 1-BB83. The Ohio State University component of the study is supported by NASA's Lunar Advanced Science and Exploration Research (LASER) Program (Grant No. NNX11AC53G). We acknowledge the SELENE project of the Japan Aerospace Exploration Agency (JAXA) and the Chang'e-1 project for providing the lunar data products used for this study. We are also in debt to two anonymous reviewers for their thoughtful reviews.

References

Araki, H., S. Tazawa, H. Noda, Y. Ishihara, S. Goossens, S. Sasaki, N. Kawano, I. Kamiya, H. Otake, J. Oberst, C.K. Shum, Lunar Global Shape and Polar Topography Derived from Kaguya-LALT Laser Altimetry, Science Vol. 323, pp. 898-900, (2009).

Archinal, B.A., Rosiek, M.R., Kirk, R.L., and Redding, B.L., The Unified Lunar Control Network 2005:

U.S. Geological Survey Open-File Report 2006-1367, http://pubs.usgs.gov/of/2006/1367/,(2006).

Bills, B. G., and Ferrari, A. J., A harmonic analysis of lunar topography, lcarus 31, 224-259. (1977).

Bills, B. G., and F. G. Lemoine, Gravitational and topographic isotropy of the Earth, Moon, Mars, and Venus, J. Geophys. Res., 100(E12), 26,275—26,295, (1995).

Davies, M.E., Colvin, T.R., and Meyer, D.L., A unified lunar control network: the near side, JGR. 92, 14177-14184, (1987).

Iz H.B., C.K. Shum, Y.Q. Chen, C.L. Dai, Improved Geometric Lunar Figure from CHANG'E-1 and SELENE Laser Altimetry (to be published in in the Journal of Applied Geodesy October 2011 issue).

iz H.B., C.K. Shum, X.L. Ding, C.L. Dai, Orientation of the Geometrically Best fitting Triaxial Lunar Ellipsoid with Respect to the Mean Earth/Polar Axis Reference Frame, Journal of Geodetic Science, 1(1) pp 52—58, (2010)

iz H.B., New Parameters of Geometrically Best Fitting Lunar Figures, Journal of Applied Geodesy Vol. 3, pp. 155—162 (2009).

Iz H.B., Y.Q. Chen, B.A. King, X.L. Ding, C. Wu, Deformation Analysis of the Unified Lunar Control Networks, Journal of Applied Geodesy, Vol. 3, pp. 231—238, (2009).

JAXA, https://www.soac.selene.isas.jaxa.jp/
archive/index.html.en(2009).

Kaula W. M., G. Schubert, R. E. Lingenfelter, W.L. Sjogren, W.R. Wollenhaupt: Lunar Topography from Apollo 15 and 16 Laser Altimetry, Proc. Lunar Sci. Con 3, 2189-2204, (1972).

Nyrtsov M.V., Geographical maps of small celestial bodies: the styles and methods of presentation, the ways of use,



^{*} Clementine best fitting three-axial solution with orientation, but without center of figure parameters (Smith et al. 1997).

Proceedings of the 22st International Cartographic Conference (ICC) A Coruña Spain ,"Mapping Approaches into a Changing World" CD-ROM ISBN: 0-958-46093-0, (2005)

Ping J., H. K., Heki, K., Matsumoto, and Y. Tamura, A Degree 180 Spherical Harmonic Model for the Lunar Topography, Adv. Space Res. Vol. 3 1, No. 11, 2377-2382, (2003).

Ping J, Q Huang, R. SHU, J. Yan, Lunar Topography Result from Chang'E-1 Laser Altimetry Mission, Presented at the 3rd KAGUYA(SELENE) Science Working Team Meeting, Tokyo, (2009).

Sjogren, W.L. and W.R.Wollenhaupt, Lunar Shape from Apollo 16 Altimeter, Science 179, 275-278, 1973.

Smith, D. E., M.T. Zuber, G. A. Neumann, and F. G. Lemoine,

"Topography of the Moon from the Clementine LIDAR," JGR, 102, no. E1, 1591—1611 (1997).

Stooke P.J. and C.P. Keller, Map projections for non-spherical worlds/ the variable-radius map projections, Cartographica 27 (2) (1990), pp. 82—100.

Wieczorek M.A., B.L. Jolliff, A. Khan, M.E. Pritchard, B.P. Weiss, J.G. Williams, L.L Hood, K. Kevin Righter, C.R. Neal, C. K. Shearer, I.S. McCallum, S. Tompkins, B.R. Hawke, C. Peterson, J.J. Gillis, B. Bussey, The Constitution and Structure of the Lunar Interior, Reviews in Mineralogy & Geochemistry, Vol. 60, pp. 221-364, 2006.

